DEVELOPMENT OF A CHARGED PARTICLE THICKNESS GAUGE

by
M. Onur Uzonur

B.S. in M.E., Istanbul Technical University, 1985

Submitted to the Institute for Graduate Studies in Science and Engineering in partial fulfillment of the requirements for the degree of

Master of Science

in

Nuclear Engineering

Boğaziçi University
1989

ACKNOWLEDGEMENTS

I would like to express my gratitude to Prof.Dr. A. Nezihi Bilge, my thesis supervisor, for his continual guidance throughout this work. Also special thanks are due to Levent Akın, Doç. Dr. Vural Altın and Prof. Dr. Turan B. Enginol for their valuable assistance, suggestions and criticism.

Onur Uzonur

ABSTRACT

The determination of the unknown sample thicknesses by using a radioactive source is one of the most widely used non-destructive measurement methods.

In this work, an attempt was made to determine the unknown thicknesses of paper sheets by using a beta source.

The components of the experimental system and their configurations were determined by minimizing the scatterings and considering physical events like the absorption of beta particles taking place in the surrounding medium.

A nonlinear curve fitting procedure was applied to the experimentally obtained data points in addition to the linear least squares method.

Errors were analyzed, interpreted and for some of the investigated cases only the source of error was located.

Finally some suggestions have been made for further work in this subject and applications in the field of on-line measurements.

ÖZET

Radyoaktif kaynak kullanımı ile bilinmeyen numune kalınlıklarının tesbiti en yaygın olarak kullanılan tahribatsız muayene metodlarından biridir.

Bu çalısmada, kağıt levhaların bir beta kaynagı kullanılarak kalınlıklarının tesbitine çalışılmıştır.

Deney sisteminin elemanlarının tesbiti ve bunların konumlandırılmaları, beta parçacıklarının sistemi çevreleyen ortam tarafından yutulmaları gibi bazı fiziksel olaylar gözönüne alınarak ve saçılmaların minimize edilmesine çalışılarak yapıldı.

Deneysel olarak elde edilen verilere doğrusal en küçük kareler metodu kullanılarak yapılan dogru uydurmanın yanısıra doğrusal olmayan en küçük karele metodu da tatbik edildi.

Hatalar analiz edilerek yorumlandı, bazı hallerde ise yalnızca hata kaynağı belirtilmekle yetinildi.

Son olarak, daha sonra yapılabilecek çalışmalar ve üretim hattı üzerindeki dinamik ölçümler için bazı tavsiyelerde bulunuldu.

TABLE OF CONTENTS

	Page
ACKNOWLEDGEMENTS	iii
ABSTRACT	iv
ÖZET	v
LIST OF FIGURES	viii
LIST OF TABLES	ix
LIST OF SYMBOLS	x
1. INTRODUCTION	1
2. THEORY	3
2.1. Modes of Decay	3
2.2. Charged Particle Spectra	4
2.2.1. Alpha Ray Spectrum and Sources	4
2.2.2. Beta Ray Spectrum and Sources	6
2.3. Charged Particle Interactions	8
2.3.1. Interactions of Electrons	9
2.3.2. Heavy Charged Particle Interactions	11
2.3.3. Specific Ionization	12
2.3.4. Alpha Straggling	13
2.3.5. Number-Distance Curve	13
2.3.6. Bragg Ionization Curve	14
2.4. Range-Energy Relations for Beta Particles	15
2.4.1. Empirical Formulas	17
2.4.2. Methods for Determining the Range	22
3. RADIATION DETECTION SYSTEMS	24
3.1. The Ionization Mechanism	24

4. EXPERIMENTAL SETUP AND PROCEDURE 30

4.1. Determination of the Components and Parameters of the System 30

4.2. Experimental Procedure 40

4.3. Determination of the Minimum and Maximum Detection Limits 41

4.4. Dynamic Effects in the Case of On-Line Thickness Measurements 45

5. UNCERTAINTIES AND NONLINEAR CURVE FITTING 52

5.1. Errors and Uncertainties 52

5.2. Nonlinear Models 53

5.2.1. Levenberg-Marquardt Method 57

5.2.2. Computational Procedure 58

6. DISCUSSION AND CONCLUSIONS 63

APPENDIX 67

REFERENCES 69

LIST OF FIGURES

Figure		Page
2.1	Alpha ray fine structure	5
2.2	Beta ray spectrum	6
2.3	Specific ionization of beta particles	12
2.4	Number-distance curve	14
2.5	Bragg curve	15
2.6	Absorption curves	16
2.7	Range-energy curve	19
3.1	The different regions of operation of gas filled detectors for two different values of particle energy	26
3.2	Equivalent counting circuit for a GM tube	29
4.1	Schematic diagram of the experimental setup	31
4.2	Calibration curve	41
4.3	Schematic diagram of a dynamic sheet	45

LIST OF TABLES

Table		Page
4.1	Determination of the collimation length	37
4.2	Determination of the detector-sample distance	38
4.3	Experimental data	43
4.4	Experimental data for the determination of the maximum range	44
5.1	Output of the non-linear curve fit	62

LIST OF SYMBOLS

A	Hessian matrix
BE	Binding energy of an electron, ev.
D	Detector response, cpm.
D_o	Detector response in the absence of a sample
E_o, E_{max}	Maximum energy of a beta spectrum, Mev.
E_{ave}	Average energy of a spectrum, Mev.
$F(y)$	Probability density function for thickness
I	Beam intensity, cpm.
I_o	Source strength, cpm.
L	Collimator length, mm.
$Q(R)$	Probability density function for count rate
R	Detector response
R_o	Maximum range, mg/cm^2.
R_e	Extrapolated range of alpha particles, mg/cm^2.
R_m	Mean range, mg/cm^2.
R_p	Practical range of beta particles, mg/cm^2.
R_u	Detector response for a uniform sheet
T	Kinetic energy, Mev.
W	Transition energy, Mev.
X_{min}	Minimum detectable thickness, mg/cm^2.
Z	Atomic number
a	Parameter vector
t	Time, sec.
u_1	Mean deviation
v	Velocity, cm/s.
w	Width of a moving sheet, cm.

x	Thickness, mg/cm^2.
$\langle y \rangle$	Average thickness, mg/cm^2.
$y(t)$	Varying thickness, mg/cm^2.
χ^2	Merit function
μ	Mass attenuation coefficient, cm^2/mg.
p	Density of sample material, mg/cm^3.
σ^2	Variance of a parameter or a function
σ_i	Statistical deviation of counts
σ_x	Uncertainty in thickness
σ_y	Uncertainty in count rate

I. INTRODUCTION

Several well known non-destructive methods to determine and control the thickness of paper sheets are widely used to increase the rate of paper production and to keep the required properties of the products uniform, during the manufacturing process. Because of their non-destructive nature, radioisotopic methods are extremely suitable for on-line thickness measurements. Measurements performed by using radioactive isotopes are easily reproducible and do not require a power supply[1]. They can also be applied to systems operating at extreme temperatures and some times these systems are the only viable ones. Due to these characteristics, such techniques have widely been used in several types of industrial applications ever since the production of radioisotopes was economically realized in large quantities in nuclear reactors.

The most important parameter in the selection of a radioisotope is the penetration capability of the particles emitted. Charged particles generally have a short range through the material because of their electrostatic charge. They can be classified as alpha particles, beta particles and heavy ions. Heavy ions have the shortest range among others. Since the alpha particles are highly charged particles, they too have a very low penetration capability. Beta particles may have comparatively long ranges depending on their source energies and the media in which they travel.

The principal methods used in thickness radio gauging are

the transmission and the back scattering techniques. In the former one, samples are placed between the detector and source. In the back scattering technique, the detector and source are placed on the same side of sample sheets so as to take advantage of backscattered particles.

In this study, a radio gauge system was constructed by using a beta particle source and employing the transmission technique.

In the design of the radio gauge system physical components were chosen and parameters were determined by considering the physical properties of the components involved and with the aim of minimizing the effects that could be disturbing the measurement process. Since a highly active radioisotope was used, a careful collimation of the detector and source proved necessary in order to prevent detector saturation. After evaluation of the experimental results, errors were statistically examined and interpreted. Finally applicability of this prototype to on-line thickness measurements was considered and suggestions were made for further work on the subject.

II. THEORY

2.1. Modes of Decay

Nuclei are stable when they contain only certain combinations of neutrons and protons. The short ranged attractive forces are balanced by the electrostatic repulsive forces in a stable nucleus. If these forces can't balance each other for some reason, the nucleus can not be stable. The number of neutrons in the nucleus has a strong effect on stability. If a nucleus contains too many neutrons, one or more of them will be spontaneously transformed into a proton, with the emission of a β^- particle and a neutrino. This phenomena is called beta decay.[2]

$$n \longrightarrow p + \beta^- + \nu \qquad (2.1)$$

If a nucleus has too few neutrons, there are two possible mechanisms by which a proton is transformed into a neutron. These are called electron capture and positron decay mechanisms.

Barrier penetration probability is related to the radius of the decay product nucleus which is greater for heavier nuclei than for others, since the barrier height decreases as the radius increases. This probability is important for α particles. A light nucleus can not emit an α particle which can penetrate out of this barrier.

All heavy nuclei are, in principle, unstable against spontaneous fission which is the only spontaneous source of

heavy charged particles heavier than α particles. However, this process is inhibited for extremely heavy nuclei, because of the large potential barrier in the distortion of the nucleus from its original spherical shape.

As a conclusion, it can be said that the decay mechanisms strongly depend on the internal structure and weight of the unstable nuclei.

2.2. Charged Particle Spectra

2.2.1. Alpha Ray Spectrum and Sources

Alpha particles are ionized helium atoms produced from radioactive alpha decay processes or from (n,α) reactions such as, $^{212}Po \longrightarrow {}^{208}Pb + \alpha$ decay or the $^{10}B(n,\alpha)\,^{7}Li$ reaction.

The kinetic energies of α particles range from about 2 to 10 MeV. There is a very strong correlation between alpha particle energy and half-life of the parent nucleus. Alpha particles with the highest energies have the shortest half-life. Only, the sources having an energy value between 4 and 6.5 MeV are usable in practice, since the utility of an alpha source is limited by its half-life.

The alpha rays from some sources are not monoenergetic but consist of several closely spaced monoenergetic groups or " alpha lines." These lines are known as " the fine structure "of alpha ray spectra." The spectrum of the α emitter

Bi^{212} points out the proximity of these lines. The energy difference between the two most energetic groups is about 40 KeV.

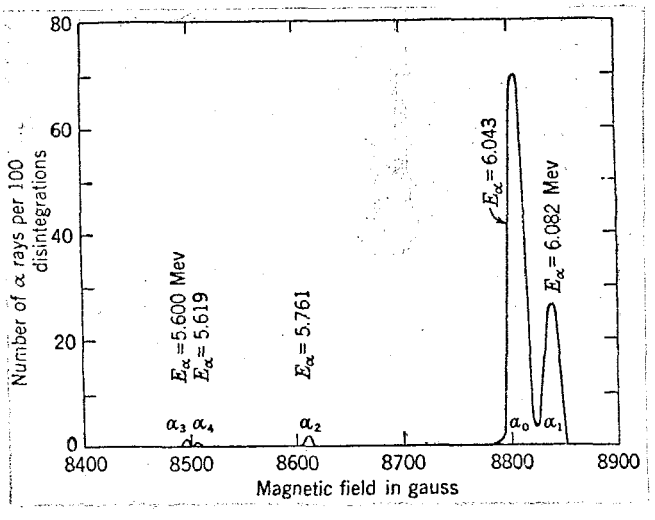

Fig.2.1. Alpha ray fine structure[2] .

In figure 2.1., "y axis" represents the number of α particles per 100 $^{212}Bi_{83} - {}^{208}Tl_{81} + {}^{4}He$ decays.

Transitions are from the ground state of the parent to the ground or the excited states of the decay product. The transition from the ground state to the ground state may not be the most intense one.

In some transitions, especially ones having a very short half-life, some of the emitted alpha particles have a longer range than the others. This phenomena is not very frequent however. These "long-range" alpha particles have a relative abundance of about ten per cent or less. Long-range alpha particles are emitted from excited levels of an alpha source, whereas the others are emitted from ground level.

2.2.2. Beta Ray Spectrum and Sources

Beta particles have a continuous spectra. A negative beta particle is called a negatron, and the positive one is called a positron. Negatron and positron decays can be considered as the transformations of one type of nucleon to another such as;

$n \longrightarrow p + \beta^- + \nu$ and $p \longrightarrow n + \beta^+ + \nu$

The existence of the neutrino in these processes can explain the continuity of the beta spectrum. Disintegration energy is shared between the emitted particle and neutrino. The residual nucleus may be left in either its ground state or an excited state.

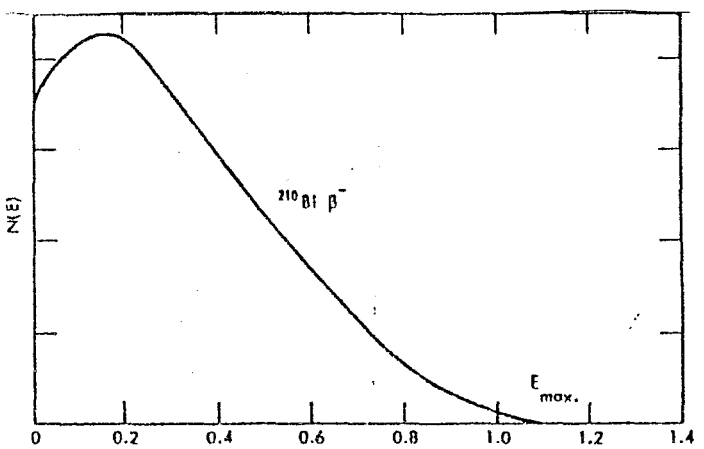

Fig.2.2. Beta ray spectrum.[3]

This is a typical beta ray spectrum. In a beta ray spectrum, the average energy of particles is about 30-40 percent of the maximum energy.

$$E_{avg} = (0.3\text{-}0.4)\ E_{max} \qquad (2.2)$$

The principle source of beta rays is β decay.

$$^{A}X_{Z} \longrightarrow ^{A}Y_{Z+1} + \beta^{-} + \nu$$

Beta particles are also produced by interactions of alpha, beta and gamma particles with matter as in the case of compton scattering, μ meson decay ($\mu^{-} \longrightarrow \beta^{-} + 2\nu$) and secondary ionization (delta rays) are some other beta particle sources.

Internal conversion, Auger electrons and thermoionization are the principle monoenergetic electron sources.

Before examining internal conversion and Auger electrons, it is better to take a look at the electron capture transitions.

If a nucleus has too few neutrons, it may capture one of its own atomic electrons and is therefore transformed to an isobar of atomic number (Z-1) and emits a mono-energetic neutrino.

$$p + e^{-} \longrightarrow n + \nu$$

In electron capture transitions the neutrinos are emitted in one or more monoenergetic groups, in contrast with the continuous distribution of neutrino energy produced in beta decay. Captured electron generally comes from the K shell and in this case a K capture is spoken of.

2.2.2.a. Auger Electrons.

Following K capture, there is an electron vacancy in the K shell. This is filled by the transition of an L shell electron into the K shell. This is followed by the emission of either a K shell X ray photon especially in heavy elements or an Auger electron especially in light elements. Energy of

the K X ray is $BE_K - BE_L$ and that of the L shell Auger electron is $BE_K - 2BE_L$.

2.2.2.b. Internal Conversion.

The transition from an excited state to a lower one can also take place without the emission of a photon. The transition energy W, can be transferred directly to a bound electron of the same atom. This phenomena is called internal conversion and in this case the kinetic energy of the ejected electron E_i is given by,

$$E_i = W - BE_i \qquad (2.3)$$

where BE_i stands for the binding energy of the ejected i^{th} shell electron.

After ejection of the photoelectron, the atom emits the energy BE_i as characteristic X rays or as Auger electrons.

2.3. Charged Particle Interactions

Charged particle interactions are primarily due to Coulomb forces.

There are four principal types of interaction by which a charged particle losses its kinetic energy or is deflected from its original path.

In an inelastic collision, the kinetic energy of the incident particle is converted to another kind of energy such as ionization or excitation, whereas in an elastic collision, it's only transferred to another particle.

2.3.1.a. Inelastic Collisions with Atomic Electrons.

Inelastic collision with bound atomic electrons is the predominant mechanism in charged particle interactions. A charged particle entering any absorbing medium interacts simultaneously with many electrons. In these interactions, an electron feels an impulse from the attractive Coulomb force as the particle passes through its vicinity. Depending on the proximity of the encounter, this impulse may either raise the electron to a higher energy level causing excitation or remove it from the atom leading to ionization.

Ionization product, called an ion pair is made of a free electron and the corresponding positive ion.

In particularly close encounters, an electron removed from its orbit may have enough energy, namely more than 1 keV, to cause secondary ionization. These electrons are called delta rays.

2.3.1.b. Inelastic Collision with a Nucleus.

In a close, noncapture encounter, a charged particle may be deflected by the nucleus. Some time during a deflection a quantum of radiation called breaking radiation or Bremsstrahlung is emitted. In this type of interaction, there is also a small probability of excitation. In other words, as a charged particle is deflected, a small part of its energy may be converted to nuclear excitation energy, while most of its energy is given off as Bremsstrahlung.

Bremsstrahlung has a continuous spectrum of X rays as opposed to the line spectrum or characteristic spectrum of

X rays given off by the electrons filling the orbits in K, L or M shells.

In Bremsstrahlung phenomena, the incident particle can radiate any amount of energy from zero upto its total kinetic energy, T.

2.3.1.c. Elastic Collision with a Nucleus.

Incident electrons have a high probability of nuclear elastic scattering. In this type of scattering a charged particle is deflected, but neither radiates nor excites the nucleus. Elastic collisions may be single or multiple. Single scattering theory is suitable for thin targets, since an incident electron does not have a chance to make another collision.

If an incident charged particle may suffer a large number of scattering collisions, then statistical methods become applicable in this case of multiscattering. Although there is voluminous work on these subjects, these theories are not easily applicable for industrial purposes.

The transfer of kinetic energy in a collision with a heavy nucleus is negligible for light particles such as beta rays.

2.3.1.d. Elastic Collisions with Atomic Electrons.

An incident charged particle may be elastically deflected by the atomic electrons of an absorber atom. The amount of energy transferred is generally less than the lowest excitation potential of the electrons, so that the interaction is really with the atom as a whole. This type of collisions are significant for the case of very low energy values less

than 100 eV and is insignificant from the point of view of industrial applications.

After the examination of four principal interaction mechanisms, another interesting phenomena related to the ionizing effect of swift charged particles can be stated. This is called Cherenkov radiation. Electromagnetic radiation is emitted whenever a charged particle passes through any medium in which the phase velocity of light is less than the particle velocity. It is independent of the rest mass of the moving particle and depends only on the charge and velocity.

In general, any incident particle may experience a number of collisions of each type. Which type of interaction will occur is determined only by laws of chance.

2.3.2 Heavy Charged Particle Interactions

While an α particle passes through the electron cloud of its own emitting atom and the neighboring ones, it will capture one or two electrons and thus become either a singly ionized or a neutral helium atom. After this capture, the swiftly moving atom will be reionized by collisions with other atoms. There is, therefore a regular electron exchange between the alpha particle and absorbing medium. This interchange becomes most rapid as the α particle velocity declines near the end of its range. For a heavy charged particle, inelastic collisions with atomic electrons is more important. The range of a proton is slightly shorter than that of an α

particle with equal energy. This can be explained using the electron exchange process mentioned above.

2.3.3. Specific Ionization

The number of ion pairs produced per unit path length of a charged particle is called the specific ionization. It is proportional to the square of the charge of the incident heavy charged particle.

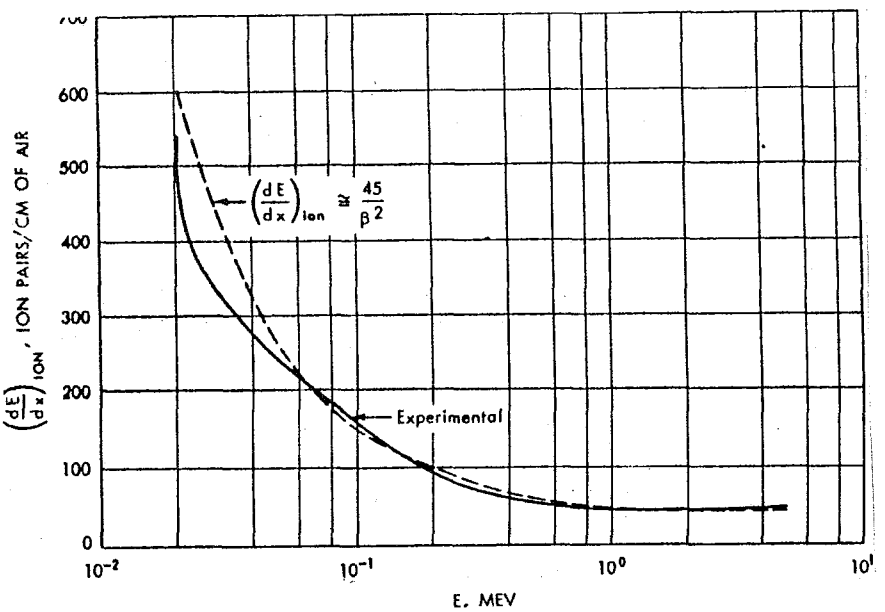

Fig.2.3. Specific ionization of beta particles.[3]

In figure 2.3. specific ionization $(dE/dx)_{ion}$ is plotted against kinetic energy E, for beta particles in air. As it can be seen from the figure, specific ionization of the highly energetic charged particles is quite low. These swift particles do not spend enough time to ionize the molecules of the surrounding material, and there is no significant amount of ionization taking place resulting in low specific ionization.

Nearly half the kinetic energy lost by an α particle is transferred in hard collisions. In a hard collision, there is a large energy transfer and the struck electron can be considered as initially free, since its binding energy is negligible in comparison with the amount of energy transferred to it. The resulting δ rays or slow electrons can produce about half the ultimate ionization.

Ionization and excitation probabilities are related to the magnitudes of respective potentials. As these potentials increase, these probabilities also increase.

2.3.4. Alpha Straggling

Identical charged particles, all having the same initial velocity, do not all have the same range. The observed ranges of individual particles from any monoenergetic source will show a normal or Gaussian distribution around the mean range. This is called range straggling.

Energy straggling refers to the variations in energy in a beam of initially monoenergetic particles after the passage through an absorber.

2.3.5. Number-distance Curve

Before the explanation of number-distance curve, it would be better to describe the mean range (R_m). It is the absorber thickness or distance in which the number of incident particles is reduced to half of its original value.

The central portion of the number-distance curve is approximately linear and an extrapolation down to the abcissa gives a value called the extrapolated range (R_e).

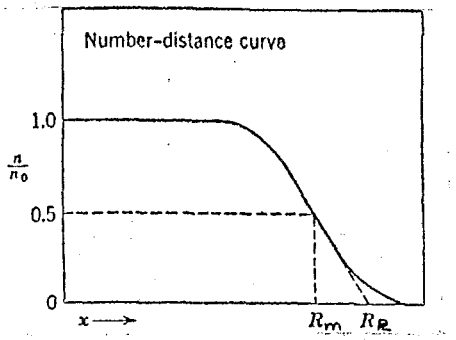

Fig.2.4. Number-distance curve.[3]

As it can be seen from figure 2.4.[3], the number of incident charged particles does not change significantly until a definite value of the absorber thickness has been penetrated through. Because of its high charge, alpha particles can not be deflected from their straight path easily until this point. After that, there is a sharp decrement because of the electron exchange pointed out above. At the end of this path, a heavy charged particle looses almost all its charge. Then, they can easily be stopped by the absorber atoms and thus there is a deviation from the straight line at the end of the curve. This deviation is caused by the increasing importance of the random collisions in this low energy state of the α particle which is by now almost neutralized.

2.3.6. Bragg Ionization Curve

The relationship between the average specific ionization and distance travelled within the target material is named

the Bragg curve. Since an average is taken over all the individual particles, this curve also includes the range straggling effect.

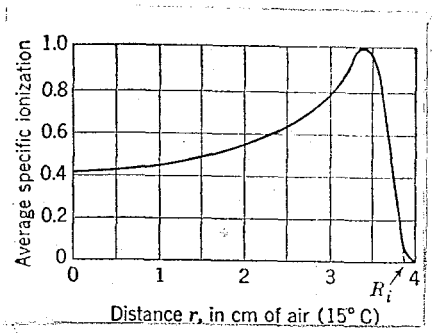

Fig.2.5. Bragg curve.[3]

The increase seen upto the peak point, may be explained as follows; while an alpha particle slows down, it can find much more time to interact with the electrons of the absorber atoms thereby ionizing much more of them while it is loosing energy.

2.4. Range-Energy Relations for Beta Particles

It is appropriate to explain some important concepts before examining the range-energy relations:

The relationship between the energy of a charged particle and its range is quite complicated and depends on several parameters which are, in general, determined experimentally.

Since beta particles are not monoenergetic, the maximum range of the particles emitted from a active isotope is determined by considering the maximum energy of the spectrum. Also, neglecting the straggling effect, it can be said that the ranges of similar particles having the same energy are

equal. So, a beta particle with the maximum energy of its spectrum has the same range as a monoenergetic electron with the same energy, since there is no physical difference between these two particles. Considering these facts, it is possible to interpret and deploy the results of experiments performed by using a monoenergetic electron source.[4]

In the intensity-thickness relationship $I = I_o \exp(-\mu x)$, "x " represents a thickness which can be considered as the range of a particle. It is also known that the range of a charged particle is an "energy dependent" quantity. Since for a given isotope, the activity does not depend on the energy of the particles emitted, the count rates denoted by I and Io can not be energy dependent. It may therefore be concluded that μ, the remaining term in this relationship, is energy dependent.

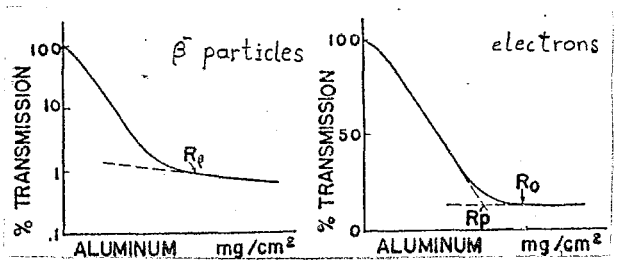

Fig. 2.6. Absorption Curves.[4]

The absorption curves for monoenergetic electrons have a long straight portion extending far into the low count rate levels. As it can be seen from figure 2.6.,[4] at the end of this portion of the curve, there is a tail going into the

background. The extension of this linear region intersects the background at some point called "the practical range" (R_p), similar to the extrapolated range described for alpha particles. The tail, described above, meets the background at a point called "the maximum range" (Ro). However, no linear region exists for beta ray absorption curves, and the definition of range is more arbitrary. Since the range of particles emitted from an isotope can not be determined accurately by inspection, some methods are used to determine the maximum range which is described in a definite way in the related method. Although, these methods are described for quite different cases, they are compatible since there is no significant difference in the ranges of monoenergetic electrons and beta particles as it was mentioned above. Also, there is no significant difference in the ranges of positrons and electrons since annihilation of positrons in flight is very rare. This is another property that makes the different methods compatible.[4]

2.4.1 Empirical Formulas

Feather's suggestion[4] for the range-energy relation may be expressed in the following form;

$$R = A \times Eo - B, \qquad (2.4)$$

where R is the range in mg/cm^2 and Eo is the energy in Mev for the case of monoenergetic electrons, or the end point energy in case of a beta spectrum. A and B are constants

given as 543 and 160, respectively, although there have been other suggested values. This expression may be applied to the energy range from 0.8 Mev to 3 Mev. However, the relationship between energy and range does not appear to be exactly linear in this interval of interest, so these values can only be regarded as being approximate.[4]

A number of researchers have proposed a different relationship between range and energy in the form

$$R = A\,E_o^{n} \qquad (2.5)$$

For the constants involved, Glocker has proposed A = 710, n = 1.72 in the energy range 0.001 to 0.3 Mev.; Glendenin and Coryell have proposed A= 407 and n = 1.38 in the energy range 0.15 to 0.8 Mev.; and Libby has proposed A = 667, n = 1.66 in the energy range 0.05 to 0.15 Mev.[4]

Katz and Penfold have used the equation

$$R(mg/cm^2) = A \times Eo^{(B - C \times \ln Eo)} = A \times E_o^{n}. \qquad (2.6)$$

The value of R at Eo = 1 Mev. was chosen as 412 mg/cm^2 and the value of n was then determined for each of the experimental points shown in Fig. 2.7 in a study by Katz and Penfold.[4] These values of n were then plotted against $\ln E_o$. The best straight line through the data values gave

$$n = 1.265 - 0.0954 \times \ln Eo$$

Thus the final equation for the range-energy relationship was

$$R(mg/cm^2) = 412 \times E_o^{1.265 - 0.0954 \ln Eo}, \qquad (2.7)$$

where the energy is in Mev. It is used for the energy levels of up to 3 Mev.

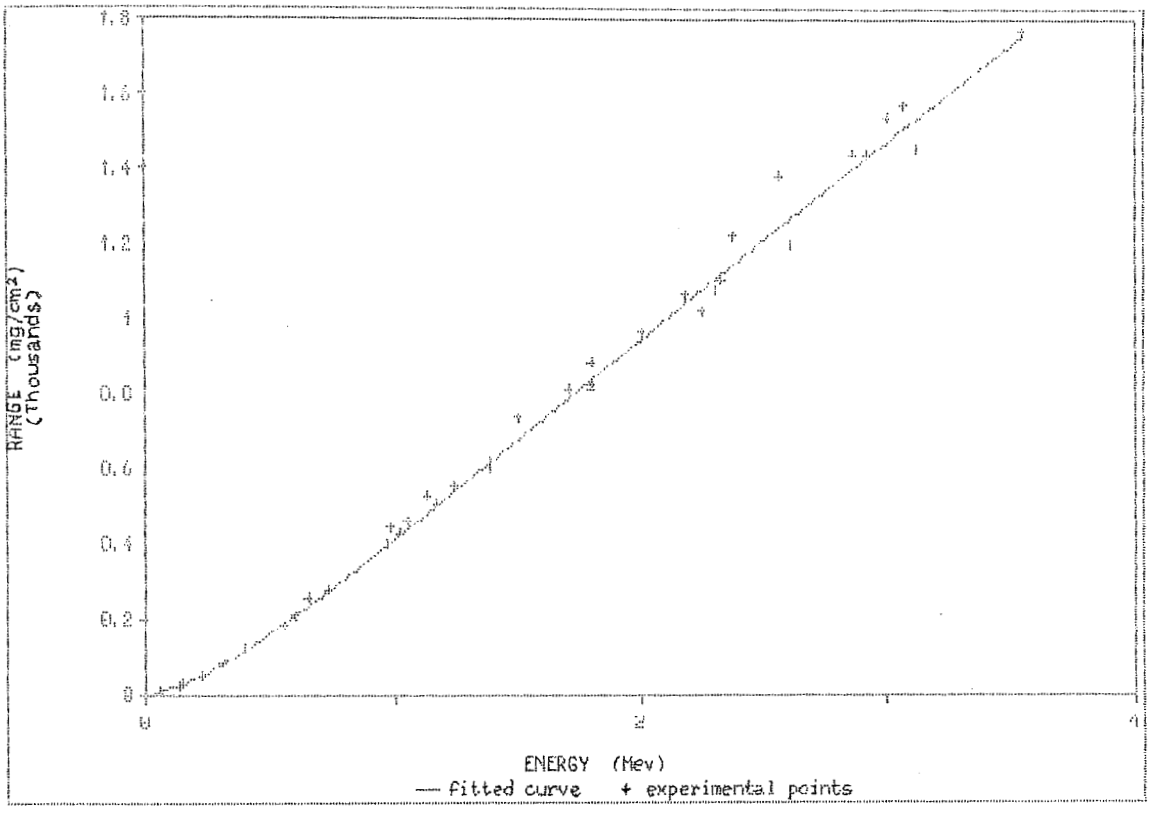

Fig. 2.7. Range-energy curve.[4]

In order to get a measure for the goodness of fit for the experimental points below 3 Mev to equation (2.7), Katz and Penfold define

$$\delta = (E_{expr}/E_{equ} - 1), \tag{2.8}$$

where E_{equ} comes from (2.7). The measure of fit may then be defined by

$$u_o = 1/N\sum_{1}^{N} \delta_i \tag{2.9}$$

with the mean and standard deviations given by

$$u_1 = 1/N \sum_{1}^{N} |\delta_i|, \qquad u_2 = [1/N \sum_{1}^{N} |\delta_i|^2]^{1/2}.$$

The range-energy curve may be represented by the following expression in the region of energies between 2.5 and 20 Mev

$$R(mg/cm^2) = 530\ Eo(Mev) - 106 \qquad (2.10)$$

In case of beta absorption, the intensity of the beam varies exponentially with absorber thickness over a limited region. Recalling equation mentioned before

$$I = Io \exp(-\mu x) \qquad (2.11)$$

where μ is the mass absorption coefficient expressed in cm^2/mg and x is the absorber thickness in mg/cm^2, the range-energy curve may be related to equation (2.11) through the following procedure. Suppose the count rate recorded for the maximum range R, is some small fraction of the initial intensity Io and is represented as $k\ I_o$, where k is a small number of the order of 10^{-4} or less depending on the sensitivity of the detector.

Then

$$k = \exp(-\mu R)$$

or

$$\mu = -\ln k / R = -\ln k / (A\ E_o^{\ n}) \qquad (2.12)$$

Some researchers give the equation

$$\mu = 22 / E_o^{\ 1.33} \qquad (2.13)$$

for energies between 0.1 and 3.0 Mev

or

$$\mu = 17 / E_o^{\ 1.43}$$

for the energy interval 0.15 to 3.5 Mev.

Recently the constants in equation (2.12) were determined as a function of Z of the absorber material by Nathuram.[5]

Another researcher, Thontadarya, determined the effect of geometry on mass attenuation coefficient of beta particles and proposed the following equations for the energy range from 0.4 to 2.3 Mev[5]

$$\mu = 16.1\ E_o^{-1.47} \quad \text{for } 2\pi \text{ geometry}$$

and

$$\mu = 17.6\ E_o^{-1.39} \quad \text{for good geometry}$$

In 2π geometry, an attempt is made to catch by the detector all the beta particles falling on the absorbers by keeping the source, absorbers and detector very close to each other.

In a good geometrical configuration both the incident and transmitted beams are well collimated and the absorbers are kept halfway between the source and detector.

Also the effect of geometry on μ values was seen to be considerable at high end-point energies above 1 Mev. Hence it is suggested that geometry of the system should be considered before any comparison of μ values is made or before using any empirical relationship to estimate μ values at the higher end-point energies of beta spectra.

By using Eqn.(2.12) for the k values indicated below, Thontadarya also derived a couple of equations relating range to mass attenuation coefficient[6];

$R = 4.606/\mu$ g/cm^2. $k = 0.01$

$R = 6.909/\mu$ g/cm^2. $k = 0.001$

2.4.2. Methods for Determining the Range

2.4.2.a Inspection Method: This is the simplest and perhaps the least reliable method. The range is determined from an inspection of the absorption curve. In order to find where the curve meets the background many accurate experimental points close to the maximum range thickness are required. If the curve approaches the background very slowly, then it is difficult to obtain good accuracy. Thick sources should be avoided since they produce slow electrons because of slowing down in the source material, thus giving rise to this difficulty. Shielding may also be needed to reduce the background effects.[4]

2.4.2.b Feather Method: In this method, absorption curve of some activity whose range is known is used as a standard for purposes of comparison with an absorption curve whose range is to be determined. After subtracting the background, the absorption curve of the standard source is divided into ten equal parts along the axis of thickness. These thicknesses are designated as;

$$d_n^\circ = Ro / n \qquad (n = 1, 2, 3, \ldots 10),$$

where Ro is the range of the standard source.

The corresponding intensities are I_n°. The ordinate of the unknown absorption curve or intensity is divided into ten parts I_n, such that $I_n = I_n^\circ$. If the thickness corresponding to I_n is d_n, then Feather assumed that

$$d_n / d_n^\circ \dashrightarrow R/Ro \quad \text{for} \quad n \dashrightarrow 10, \qquad (2.14)$$

where R is the value of the unknown range.

This method is not valid however if the absorption curves of the unknown and standard sources do not approach the end-point in a similar fashion. In spite of this weakness, this method gives fairly accurate results.

Also, some other methods have been suggested by several researchers. Some of these methods are used to determine the end-point energies rather than the range[4].

III. RADIATION DETECTION SYSTEMS

The proper selection of the radiation detection system makes the difference between an excellent application of a nuclear measurement method and a completely worthless one.

Detection mechanisms can be classified into three groups as gas detection, semiconductor detection and scintillator systems. In this chapter only the former one has been considered in detail, since it is the most suitable mechanism for charged particle measurements and is the one used in our measurements.

3.1. The Ionization Mechanism

A gas detection system is composed of three components; filled gas, electrodes, and a sealed tube covering them. The main principle of gas detection mechanism is ionization of the filling gas by radiation. The ion pairs, i.e. positive ions and electrons produced by the incident radiation, move toward their respective electrodes by the effect of an applied electric field and thus an electric current occurs. The voltage drop caused by this current is a measure of the extent of ionization[2,7].

The gas detection mechanism described above, is used in ionization chambers, proportional counters, and Geiger-Muller tubes. They are quite similar, but there are some constructional differences and they have different pressure,

gas multiplication and applied voltage values.

The electrons produced by ionization may gain enough energy between collisions to cause secondary ionizations. This phenomenon is called "gas multiplication" or "gas amplification."

There are some other important events following ionization: Positive and negative ions tend to combine and produce a photon. This is called "recombination."

It has already been stated that, only negative ions can produce secondary ionization. Positive ions can not cause a significant amount of secondary ionization since they have very short path lengths. The secondary ionization produced by positive ions can be neglected, but they can produce electrons in another way. When they are very close to a metallic surface which may be an electrode or internal metallic surface of the detector, they may pull electrons from the metallic surface. This process can be important, depending on the kind of filling gas. An ordinary gas atom can not remain excited for a long time.

Rare gas atoms have some excited states which they can occupy for relatively long periods of about 10 seconds. These are called metastable atoms. In case of pure argon being used as the filling gas, positive argon ions will find enough time to make several collisions and some eventually will pull electrons from the metallic surfaces of the detector. Adding some amount of methane to argon increases the collision probability of argon ions with methane

molecules. As a result of these collisions, argon ions will be deexcited, and methane molecules will be converted into excited methane ions that can survive as such only for a short time. They may find a chance to pull a metallic surface electron for only once. If they have some access energy, they usually loose it by collisions. Because of this property, methane and some similar gases are generally added into the detector filling gas.

Some certain gases catch a free electron and attach it to their neutral atoms. This phenomena is called "electron attachment." Argon and other inert gases have low electron attachment affinities. This is the main reason for the use of rare gases in gas filled detectors.

At this point, it might be helpful to look into some differences between gas filled detectors, considering their high voltage-count rate characteristics.

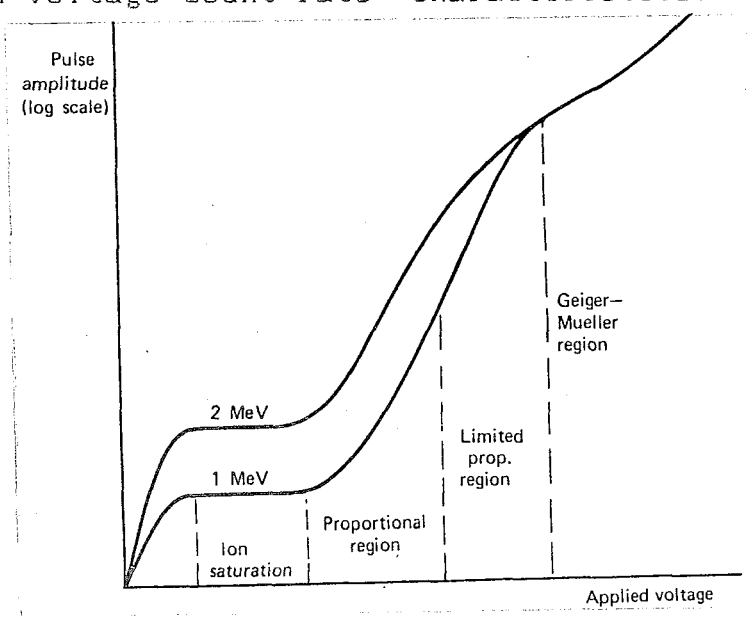

Fig.3.1. The different regions of operation of gas-filled detectors for two different values of particle energy.[8,9]

It is not possible to register any counts at the detector until a definite high voltage value is reached. Of course, there will be some ionization because of incident radiation which is independent of the applied voltage. Since ion pairs recombine easily because of the weak electric field, this region is called the recombination region.

If the applied voltage is increased, some counts are registered and this is the ionization region in which the ionization chambers work.

As it is further increased, at a definite value of the voltage, recombination effects are no longer observed and all the ions formed within the sensitive volume of the detector are collected on the anode. This is the saturation region of the ionization chamber and all the ionization chambers should ideally work in this region.

If the high voltage is increased further, ions produced will accelerate toward their respective electrodes and gain sufficient energy to cause additional ionizations. In this region, the rate of recombination is very low, and the number of pulses and the amount of energy deposited in the detector volume is proportional to the intensity of the beam incident upon the detector volume. Therefore this region is called the proportional counter region.

If the applied high voltage is increased above the proportional region, some secondary ions will gain enough energy to cause further ionizations in an adjacent region. Thus, some pulses registered will become independent of

the initial amounts of ionization. This is the limited proportionality region. In this region, photons produced by recombinations may also cause further ionizations in an adjacent region.

A further increase in high voltage equalizes this probability of successive ionizations to unity. In other words, a photon produced by a recombination event is going to cause further ionizations in an adjacent region and the resulting secondary ionization products are also going to produce further ionizations in another adjacent region. Thus an avalanche of negative ions will spread through the entire length of the center wire i.e. the anode. When a definite value of the voltage is reached, a sheath formed by positive ions will surround the center wire and reduce the potential difference below the necessary potential value for amplification and thus the discharge becomes terminated. This region is known as the GM region. In which the high voltage-count rate curve generally has a small slope and is called the GM plateau.

In the plateau region, count rate is quite independent of the applied voltage. Thus, any initial ionization produces the same discharge. Any increment of the voltage above the plateau level will cause a continuous discharge because of the positive ion bombardment of the counter wall.[10]

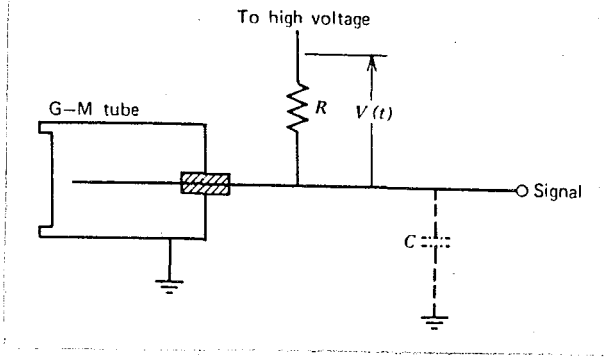

Fig.3.2. Equivalent counting circuit for a G-M tube.[7]

In figure 3.2., the diagram of a gas filled detector is shown schematically. As it can be seen from the figure, the voltage drop can be measured over a very large resistor of about 10^{12} ohms placed in series with the detector by the use of a voltmeter placed in parallel with the circuit. This voltage drop is a measure of the ionization current flowing through the circuit.

This current may also be measured directly by using an amperemeter placed in series with the circuit.

IV. EXPERIMENTAL SETUP AND PROCEDURE

4.1. Determination of the Components and Parameters of the System

The major aim of this work is to determine the thickness of paper sheets using a charged particle source.

Theoretical base of the study is the physical relation which can be expressed as,

$$I = I_o \exp(-\mu x) \qquad (4.1)$$

where, I_o is the intensity of the collimated beam, and I is the intensity observed after a definite thickness of the sample, both of which can be measured by a count rate meter. It is clear that, all the measurements must be performed in a limited time, since attenuation should be observed for a certain period of time. "x " is the thickness of the sample in centimeters, and μ is the attenuation coefficient of the paper medium in cm^{-1}. Multiplying the thickness x, and dividing μ by p, namely the density of the target material gives the most common form of the equation stated above. "x" now stands for the mass of a unit area of the target material [g/cm^2], and is renamed as "mass thickness." Similarly μ has the dimension cm^2/g, and is called "the mass attenuation coefficient." Also, it is well known that the detector output signal must be amplified before reading it out at the rate meter.

As it has been mentioned, components of the system are determined by the physical parameters to be measured such as the count rate, and the accumulation time needed. Therefore in such an experiment physical components of the setup that will be used are quite definite. An amplifier, a rate meter and a timer become the essential components of this kind of a system.

During the measurements, the coarse and the fine gain levels of the amplifier were set at two and three, respectively. Those are the minimum possible gain values.

The type of the detector depends on the kind of source (i.e. α, β or γ) to be used. Whereas, the type of source is determined by the sample that will be employed as target material. For the measurements that are performed with charged particles, the use of a G.M. tube is almost mandatory, because of the properties of this type of detectors already explained in chapter 3. In the measurements a "one inch" GM detector is used.

The schematic diagram of components of the experimental system is shown in Fig. 4.1.

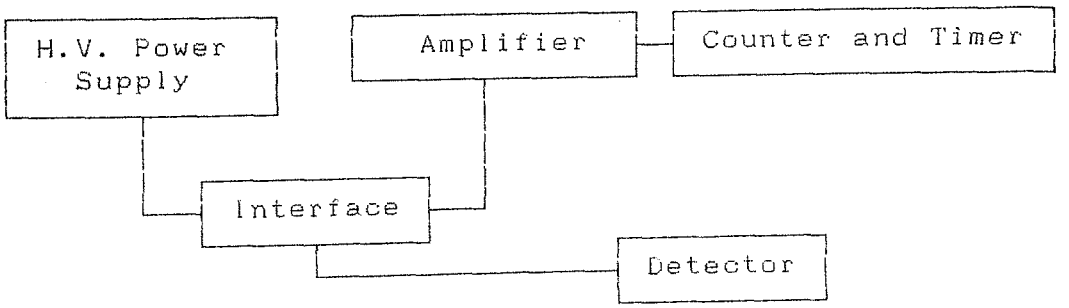

Fig. 4.1. Schematic diagram of the experimental setup.

As a first step in the determination of system configuration and component characteristics, source to detector distance is experimentally determined. In general, an appropriate count rate level is chosen in order to have a sufficiently small standard deviation considering the discriminative capability of the detection mechanism. After that, the source-detector distance is varied until this count rate is attained by taking advantage of the inverse square law.

During the experiments, the Geiger-Mueller tube was saturated because of high source activity, and thus the inverse square law could not be observed in the rate meter. Clearly no measurements could be performed in this region. In order to remedy this undesirable situation two possible approaches could be employed which are redetermination of the source-detector distance and a reduction of the strength of beta particle beam with a thick absorber. The former is the simplest and the most effective way to reduce the count rate and therefore the source is removed further from the detector. There is a limitation of this approach however which is that if source to detector distance is greatly increased without sealing the setup in a vacuum tube, the incident beam of beta particles may interact with the surrounding air so as to distort the inverse square law. Since the measurements are relative, meaning the important quantities are the count rates with and without the target material, this effect may not be very important but, an

additional uncertainty in the form of an extra source of error, however slight, would be undesirable.

As it was pointed out, the incident beam can be collimated and also the count rate can be reduced by placing a thick collimator in front of the source. An orifice with a small diameter performs this work satisfactorily. So, the effective area of the source can be reduced by appropriately adjusting the diameter of the collimator until the desired count rate is observed. This method too has a limitation, because it is well known that the efficiency of a G.M. tube for γ ray photons is quite low, since they may penetrate through the tube without any interaction. The same thing can not however be said for the X-ray photons and most G.M. tubes are quite sensitive to X-rays. A careless choice may result in undesirable additional counts due to the X rays induced in the collimator material by the beta particles. However, use of a very thick absorber would reduce this effect by self absorption. Also, in the experiments most of the induced X-ray photons can not reach the detector, because of the possible interactions on the way. Use of a very thick non-metallic absorber-collimator may be another way to avoid X-rays.

In the light of theseconsiderations variation of source to detector distance was chosen to reduce the count rate and the ideal source detector distance was determined as 40 centimeters for the experimental prototype system.

After this step, the appropriate collimator size was determined by using several collimator materials and changing the collimation length for each collimator material.

Initially, there were four parameters to be considered; collimator diameter, collimation length as given by the length of the collimator, collimator material and thickness. To determine suitable values for these parameters, three of them were fixed and the remaining one is varied to observe its effect on the results.

Clearly it would be improper to use a collimator having a diameter smaller than the diameter of the detector window, since this would reduce the effective area of the detector. On the other hand, a diameter larger than that of the detector would mean no effective collimation.

Actually, in such an experiment, the collimator located on the source side might have the major effect in comparison with the one on the detector side, whose effectiveness depends on the geometry of the system. In consideration of this, it was decided that any diameter could be chosen for the collimator on the detector side. Since the collimators used were designed as small cylindrical annuli for simplicity, and the detector used is a cylindrical one, it was decided to roll the collimator sheet over the cylindrical surface of the detector. It thus became possible to easily fix the collimator on the detector, but in this case collimation effect proves to be quite weak and it can be said that only a small fraction of the

particles scattered in the direction of the detector will be eliminated. Under these conditions, the diameter of the collimator on the detector side is equal to the diameter of the detector, and it is slightly larger than the diameter of the detector window.

Similar arguments hold for the collimator located on the source side namely that too large a diameter can not collimate the beam well and too small a diameter has the drawbacks mentioned above. Although, it is possible to reduce this kind of effects, it was decided to use a collimator whose diameter is roughly equal to the diameter of the source (≈ 15 mm.).

After the determination of collimator diameters, a metallic collimator made of cadmium was tested to determine the effect of the thickness of collimator material. A few collimators having different annular thicknesses were produced. It is observed that, increasing thickness value does not produce a significant effect as expected, since the particles scattered in the radial direction probably will not be scattered back into the detector.

After this step, several materials including paper, cadmium, copper, and thin lead sheets were tested as collimator materials. It was observed that, there is no significant difference between the metallic collimators having the same geometric configuration, despite their different Z values.

Considering these factors, a copper sheet of 1.2 mm. thickness was used to make a cylindric collimator.

The length of the collimator needs to be determined as the last parameter related to the collimation process. Some of the previously obtained results have been used to determine this parameter. Firstly, material effects and sheet thicknesses had been found to be not very important so long as similar materials such as metals are used. Of course, a paper collimator, i.e. a very light collimator with a very low Z value may give different results from the ones obtained by using a cadmium collimator with a very high Z value. But, it is possible to neutralize these effects. For example, an 11 mm. thick paper collimator may give the same collimation effect as a 1.2 mm. thick cadmium absorber. In other words, the same probability of scattering of the particles toward the detector can be maintained by increasing the material thickness in case a lower Z collimator material is used.

Considering these factors, it was decided to use thick paper collimators to determine the collimation length. This kind of collimators were prepared in the laboratory in a modular fashion so that lengths sufficient to prevent the scattering effects could easily be put together. The length of each individual collimator pipe being denoted by L (L = 57.3 mm.), measurements were performed for 2L, 3L, and 4L collimation lengths, and proper collimation length was attempted to be determined by linear interpolation. The

proper collimator length was chosen as the length that would give a 30 to 40 per cent reduction in count rates. So, it would be possible to obtain a good collimation without drastically attenuating the intensity. The proper collimator length was seen to be quite close to the initial collimator length, L, and thus a collimator length of L was decided upon. Results of these measurements are given in table 4.1.

After that, considering the difficulties that would be caused by the use of a paper collimator which is very hard to standardize, cadmium was chosen as the collimator material. The percent decrement indicated in table 4.1. is the reduction in count rate because of the use of a collimator, and it is calculated as;

$$\text{percentage decrement} = \frac{(I_o - I)}{I_o} \times 100 \qquad (4.2)$$

where, I_o is the source strength given by zero collimation length.

Table 4.1. Determination of the collimation length.

Collimation Length (mm.)	Count Rate (c.p.m.)	Decrement (%)
0	519313	-
57	369568	28.83
114	274532	47.10
171	234162	54.90
228	243212	53.20

Another parameter that needs to be determined is the dis-

tance either between the source and the sample or between the sample and the detector. The first step in determining this distance is the measurement of the strength of collimated beam, Io, and then placing the sample holder without an absorber at several positions along the source-detector line of sight so as to record the respective count rates. Of course, there will be some disturbances in the count rate because of the sample holder placed between the source and detector. The position of minimum disturbance in count rate will point out the appropriate position for the sample holder. The result of this measurement is in table 4.2.

Table 4.2. Determination of the detector-sample distance.

Sample Distance from the Detector (cm)	Reduction in Count Rate (c.p.m.)
1	1045
10.5	2626
30	1947

The count rate differences are shown on the right hand side column of table 4.2. and are obtained by subtracting the source strength, Io, from the count rate observed at a definite distance. The source strength in our case is about 1.9×10^5 counts per minute.

According to Table 4.2. the most appropriate position is obtained when the sample holder is located very close to the detector, therefore the sample holder has been positioned at a distance of 1 cm. from the detector.

Also, it should be noted that all the differences are

positive. Although, it is expected that the sample holder may cause some absorption, it can be concluded that the scattering interactions are much more effective than the absorptions. In any case, the location of the sample holder was chosen so as to minimize its effect on the count rate. However, it is seen that the minimum count rate difference is higher than σ ; the statistical deviation at this count rate level of about 1.9×10^5 cpm. This may be an important source of error. According to the experimental procedure, the source strength in the presence of sample holder is determined first, and it includes some additional counts caused by the scatterings mentioned above. After that, samples are placed into the source holder one by one. As the mass thickness of the sample is increased, some of the particles scattered back by the sample holder will be absorbed in the sample material, and the effect of these scatterings may not be observed after a definite mass thickness value. Thus, an effect that is observed at the beginning of the measurements with low sample thicknesses will decrease as the thickness gets larger and larger. In this experiment, the sample holder was made of a plastic material in the form of a frame keeping the samples together tightly, and preventing the occurrence of air cavities among the sample layers. A thick frame is much more appropriate to compress the sample layers tightly, but this would mean that the area of the sample holder will be increased resulting in a rise in the number of scatterings. This problem could be alleviated by

changing the sample holder. Clearly, a large and thin frame made of a light material is the most appropriate to reduce the effect of scatterings. However, in this case, it would be very difficult to prevent bending and to keep the samples tight since the samples used in these measurements are made of paper.

As a result, some additional counts produced by the scatterings taking place at the surfaces of the scaled box are registered by the present system, but a scaled box makes the measurement procedure very easy and is therefore not dispensable. Also, in this way the structure of the setup is rigid and more compact. In the light of these points, it was decided to preserve the structure of the system and consider this effect as a source of error. The interpretation of this error will be examined in chapter related to the subject.

4.2. Experimental Procedure

Thickness measurements can only be performed after determination of the system parameters. During the experimental procedure firstly, absorbers with different mass thicknesses are placed in a scaled box, and count rates are recorded and then, using mass thickness and count rate data values a calibration curve is obtained as it is seen in Fig.4.2.

As the final step, an unknown mass thickness value is determined using the observed count rate for this thickness and the calibration curve. For this purpose a numerical procedure is employed rather than performing an interpolation

on the graph. Thus, unknown thickness values are computed by the use of experimental data, directly and this numerical procedure will be explained in a related chapter.

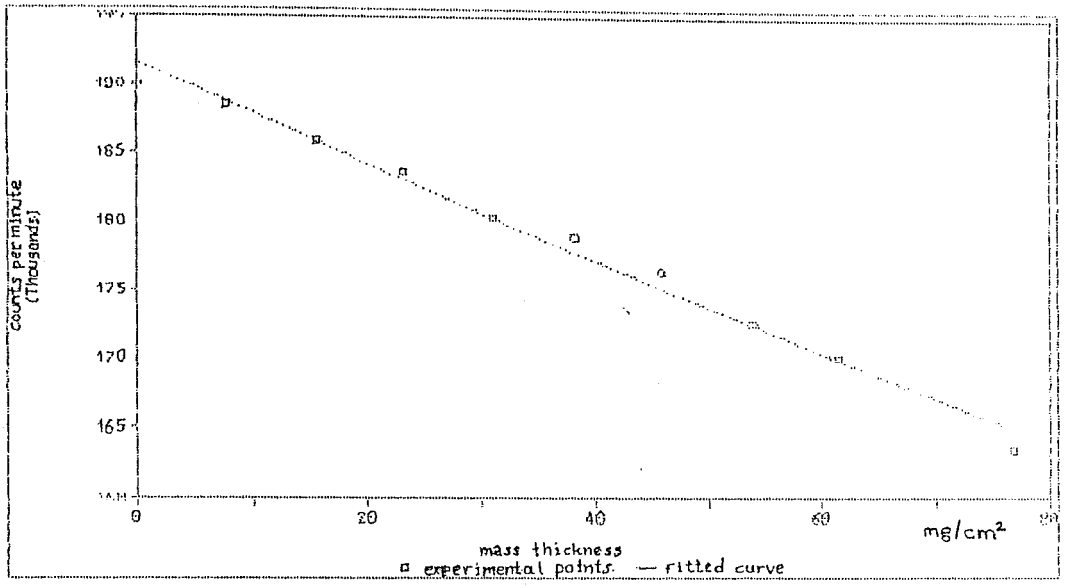

Fig. 4.2. Calibration Curve.

4.3. Determination of the Minimum and Maximum Detection Limits

In such a measurement, determination of the minimum and maximum detection limits are very important. The minimum detection limit referring to the minimum detectable thickness value can be computed theoretically as follows:

Firstly I_o, the strength of the collimated beam, is determined as described above. It is the count rate registered without any sample i.e. for zero thickness. The minimum detectable mass thickness value must give a count rate which is one standard deviation lower than Io. Other-

wise, it can not be detected, because this count rate is within the range of statistical fluctuations of I_o. So, the count rate which gives the minimum detectable thickness is:

$$I(Xmin) = I_o - \sigma(I_o) \qquad (4.3)$$

inserting this into Eqn.(4.1) gives,

$$I_o - \sigma(I_o) = I_o \exp(-\mu x)$$

considering that the standard deviation is roughly equal to the square root of the number, dividing each side by I_o, and rearranging gives;

$$x = -\ln \left(1 - \frac{1}{\sqrt{I_o}} \right) / \mu \qquad (4.4)$$

In the experimental measurements performed with a highly energetic source and a very light sample such as paper, the results are somewhat different from the theoretical ones because of weak attenuation. For the experimental setup, the use of a very energetic Sr^{90} source (2.24 MeV.) for quite low thickness values is the reason for this deviation. Also, some differences in chemical composition and humidity of the samples implying different density and mass attenuation coefficient values may cause some errors which make it difficult to obtain a value very close to the theoretical minimum one. To prevent this, all the sample sheets must be kept under similar conditions. The temperature and especially the humidity of the samples must be fixed. To fix the chemical composition of the samples, all the sample sheets should be obtained from the same large sample sheet. However, to obtain very thick samples, it is necessary to use many

layers of this paper together. This very thick absorber changes the geometric configuration of the system, and causes some additional scatterings. This effect will be explained later.

As stated above, the minimum experimentally detectable thickness is slightly larger than the theoretical one. Through the use of the results of measurements given in Table 4.3. this was found to be approximately 1.8 mg/cm^2.

Table 4.3. Experimental data.

Mass Thickness (mg/cm^2)	Count Rate (c.p.m.)
0	365820
2.29	365121
5.88	363424
8.82	363077
11.76	362101
14.71	361133
20.59	358732
23.53	357486

The thick samples are needed especially, for measurements of the maximum range. So, if the sample material is very light, as is the case under consideration, then the samples used to determine the maximum range or the maximum detectable thickness will be very thick. Of course, in this case some changes, however slight, in the geometry of the system and the collimated beam will have taken place. The scatterings do not permit the count rate to fall as low as the background level. So, it can be concluded that the maximum range of particles emitted from this beta source in a sample material

can not be observed because of the scatterings. Of course, this conclusion is valid for only similar experimental systems. A well collimated beam, a sealed tube that minimizes these scatterings, and a shield covering the whole system would make the determination of the maximum range possible. The theoretical and experimental studies on the maximum range determination has been given in the second chapter.

Under these conditions, it could only be possible to determine the experimental range of 2 MeV. beta particles, instead of the actual maximum range where the count rate is reduced to the background level. Our experimental calibration curve decreases exponentially to a definite count level but not to the background level because of undesirable scatterings. A further increase in mass thickness would not cause a significant decrease in the count rate. This count rate gives the experimental maximum range in a definite material. According to the measurements, it was calculated to be about 987 mg/cm² for the samples made of cardboard, considering the values given in table 4.4.

Table 4.4. Experimental data.

Mass Thickness (mg/cm²)	Count Rate (c.p.m.)
0	188196
216.1085	96136
323.6198	55968
431.0201	30647
538.6102	14262
648.6671	5588
756.5404	2014
871.9250	990
987.3096	794
1096.7970	792

The results of the measurements, experimentally obtained data and their calibration curves are given in the Appendix.

4.4. Dynamic Effects in the Case of On-line Thickness Measurements

An important feature of the mass thickness measurements through the use of radio-gauges is the ability to measure the parameters of the system continuously, without disturbing it during the measurement process. But experimental observation time during the measurements is quite limited because of the moving sample sheet. Nevertheless, this is not an undesirable situation for non-uniform sheets, since it reduces the area of the region being examined. Obviously, an average taken over a smaller area, represents the properties of the region better than the one taken over the whole sheet. As it was stated before, the degree of surface irregularity may contribute to the error in the measurement. The incident beam width and the velocity of the moving sheet are then some of the parameters affecting the accuracy of the measurements. There are also some instrumental sources of error associated with radiation source fluctuation and detector dead time.

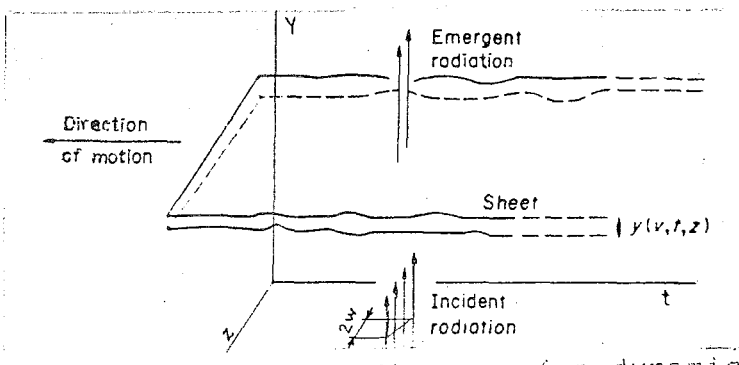

Fig. 4.3. Schematic diagram of a dynamic sheet.[11]

For a time independent monoenergetic beam of radiation crossing a moving sheet as shown in Fig. 4.3., the detector response during a time interval τ, is[11]

$$R = \frac{1}{2w\tau} \int_{-w}^{w} \int_{0}^{\tau} R_0 \exp[-\mu \rho\, y(v,t,z)]dt\, dz \qquad (4.5)$$

where all the symbols are used with their usual meanings or as shown in Fig. 4.3. Also it is assumed that the sheet is moving with a constant speed, v, as is customarily done in practice. For a uniform sheet, detector response becomes

$$\begin{aligned} R_u &= \frac{1}{2w\tau} \int_{-w}^{w} \int_{0}^{\tau} R_0 \exp[-\mu \rho\, y_u]dt\, dz \\ &= R_0 \exp[-\mu \rho\, y_u] \end{aligned} \qquad (4.6)$$

where y_u is the thickness of the uniform sheet.

The mean thicknesses corresponding to equations (4.5) and (4.6) are respectively

$$\langle y(v,t,z)\rangle = \frac{1}{2w\tau} \int_{0}^{\tau} \int_{-w}^{w} y(v,t,z)dz\, dt \qquad (4.7)$$

and

$$\begin{aligned} \langle y_u \rangle &= y_u \\ &= \frac{1}{\mu \rho} \ln(R_0/R_u) \end{aligned} \qquad (4.8)$$

The fractional error is described as

$$|\langle y(v,t,z)\rangle - \langle y_u \rangle| \;/\; \langle y(v,t,z)\rangle \qquad (4.9)$$

These equations had been evaluated for several irregular cases such as square-wave shape thickness variations and linearly increasing thickness along the direction of motion

or in the perpendicular direction by Oyedele[11]. Although the results change from one case to another, there are some common points which may be summarized as follows: The error increases with the degree of surface irregularity, as it is expected. In most systems, the error is larger when the thickness variation is in both directions i.e. along the direction of motion and perpendicular to it, than when it is only in one direction. Also, the use of lower speeds and shorter measurement time intervals as well as narrower beam widths reduce the error in most systems. The use of lower speeds allows a detection system to perform much more precise measurements as in the case of static radio-gauging. The speed of the sample sheet is generally determined by the production process onto which on-line thickness measurement is applied. It is clear that the lowest possible speed value must be chosen to reduce the error mentioned above. With the use of a shorter time interval and a narrower beam, it is possible to perform measurements over a smaller area. This minimizes the effect of irregularities since all the data are collected from a small region. However, the time interval must be long enough to reduce the error due to the statistical variation of data.

To consider the source fluctuation effect in continuous radio gauging, the detector response can be expressed as[12]

$$D = \frac{D_o}{\bar{I}_o \tau} \int_o^{\tau} I_o(t) \exp[-\mu \rho y(t)] \, dt \qquad (4.10)$$

where, $I_o(t)$ is the intensity of the beam incident on a sheet

having a thickness $y(t)$ and D_o is the detector response in the absence of the sheet. The average intensity I_o is determined by observing D_o over a sufficiently long time interval.

The detector response reduces to the following form for the case of uniform thickness and constant intensity.

$$D_u = \frac{D_o I_o}{\bar{I}_o \tau} \int_o^\tau \exp[-\mu \rho y_u .] \, dt$$

$$= D_o \exp[-\mu \rho y_u .] \qquad (4.11)$$

and using

$$T_u . = D_u . / D_o = \exp[-\mu \rho y_u .] \qquad (4.12)$$

where the subscript u' indicates uniform thickness and time independent incident beam intensity. The corresponding average thickness is

$$\langle y_u . \rangle = \frac{1}{\tau} \int_o^\tau y_u . \, dt \equiv y_u . \qquad (4.12.1)$$

If source fluctuation and thickness variation are taken into account then,

$$T = D/D_o = \frac{1}{\bar{I}_o \tau} \int_o^\tau I_o(t) \exp[-\mu \rho y(t)] \, dt \qquad (4.13)$$

and

$$\langle y(t) \rangle = \frac{1}{\tau} \int_o^\tau y(t) \, dt \qquad (4.14)$$

are found as expressed above. If $\langle y_u . \rangle$ and $\langle y(t) \rangle$ are not the same, then there is an error in the calibration process given by,

$$\Delta y = \langle y(t) \rangle - \langle y_{u.} \rangle \qquad (4.15)$$

It is possible to equate equations (4.12) and (4.13) according to the following arguments; Firstly, the measurements are performed by using the assumption of uniform thickness and constant source intensity, as usual. After that, the data which have been obtained and the model for the surface irregularities are considered to determine the effect of the irregular surface and source fluctuation. It is clear that, in this case the response of the detector does not change since the expressions are evaluated for the same data. In other words, D and T are equal to $D_{u.}$ and $T_{u.}$ respectively. Equating $\langle y_{u.} \rangle$ and T by setting equations (4.12) and (4.13) equal to each other,

$$y_{u.} = -\frac{1}{\mu\, p} \ln\left[\frac{1}{\bar{I}_o \tau} \int_o^{\tau} I_o(t)\, \exp[-\mu\, p\, y(t)]\, dt\right] \qquad (4.16)$$

substituting into equation (4.15) gives

$$\Delta y = \langle y(t) \rangle + \frac{1}{\mu\, p} \ln\left[\frac{1}{\bar{I}_o \tau} \int_o^{\tau} I_o(t)\, \exp[-\mu\, p\, y(t)]\, dt\right] \qquad (4.17)$$

which is the error in the on-line sheet thickness calibration for the case of source fluctuation.

The incident intensity $I_o(t)$ in equation (4.17) is, in general, specified by a probability density function and the corresponding error y may be specified by another probability density function. Setting

$$r(t) = (I_o(t)\, \exp[-\mu\, p\, y(t)])/(\bar{I}_o \tau) \qquad (4.18)$$

and

$$R(\tau) = \int_0^{\tau} r(t)\, dt \qquad (4.19)$$

equation (4.17) becomes

$$y = \langle y \rangle + [\ln R(\tau)]/ \mu \rho \qquad (4.20)$$

so that

$$F(\Delta y)\, d(\Delta y) = Q(R)\, dR \qquad (4.21)$$

where $F(y)$ and $Q(R)$ are the probability density functions for y and R respectively. If a Gaussian distribution is chosen for the probability density function of the incident intensity $I_o(t)$, then $r(t)$ and $R(\tau)$ will also be Gaussian for a given thickness, $y(t)$. Their mean values are

$$\mu_r = \exp[-\mu \rho\, y(t)]/\tau \qquad (4.22)$$

and

$$\mu_R = \frac{1}{\tau} \int_0^{\tau} \exp[-\mu \rho\, y(t)]\, dt \qquad (4.23)$$

with the variances

$$\sigma_r^2 = \sigma_o^2 [\exp(-2 \mu \rho\, y(t))]/(\bar{I}_o \tau)^2 \qquad (4.24)$$

and

$$\sigma_R^2 = \frac{\sigma_o^2}{(\bar{I}_o \tau)^2} \int \exp[-2 \mu \rho\, y(t)]\, dt \qquad (4.25)$$

The probability density function for R can be written as

$$Q(R) = \frac{1}{\sqrt{2\pi}\sigma_R} \exp[-(R-\mu)^2/2\sigma_R^2] \qquad (4.26)$$

Substituting this in equation (4.21) and using eqn. (4.20)

$$F(\Delta y) = \frac{\mu \rho}{\sqrt{2\pi\sigma_R^2}} \times [\exp-(\exp[\mu \rho(\Delta y - \langle y \rangle)] - \mu_R)^2 / 2\sigma_R^2] \times \exp[\mu \rho(\Delta y - \langle y \rangle)] \quad (4.27)$$

Equation (4.27) gives the probability density function for the error y and for thickness y(t), when the probability density funtion of the incident intensity is Gaussian. As it is seen from equation (4.27) the values of $F(\Delta y)$ depend on the thickness variation.

Equation (4.27) have been evaluated for different sheets as an application by Oyedele.[12] Consequently, it was suggested that a radiation source whose probability density function has a small variance is the most suitable for continuous radio gauging since the variance of the probability density function for the error increases with that of the incident radiation.

Also, the dead time of the detection system is quite important for dynamic measurements. Clearly, a larger dead time is undesirable. If τ is very large, the response of the system at the time considered may not represent the quantity being examined since it indicates a value belonging to a previous point in time. However, a larger τ reduces the standard deviation of counts since it separates the measurements and prevents the effect of previous measurements. So it can be concluded that the dead time of the system must be sufficiently small to make the dynamic measurements possible.

V. UNCERTAINTIES AND NONLINEAR CURVE FITTING

5.1. Errors and Uncertainties

The experimental procedure followed provides a data set formed for modelling the system. However, the data are not exact and are subject to measurement or statistical errors. Thus, generally data do not fit the model exactly, even if the model used is the appropriate one[13]. The determination of such errors is quite important in quantitative interpretation of measurements. Measurement errors can be classified into three major groups. These are reading errors, round off errors, and truncation errors. In some measurement systems such as digital rate meters, it seems that there is no reading error, but measured values are rounded off or truncated by the system because of the physical difficulties or sensitivity limits.

Statistical errors may be caused by the physical properties of the system under examination. For example, the process of nuclear decay is a statistical phenomenon and therefore, the measurements performed to determine the decay rate shows a statistical distribution. Statistical errors show a definite distribution which may be a normal, binomial or a Poisson distribution depending on the physical properties of the system. Nuclear phenomena, generally show a Poisson distribution but only the normal distribution is being examined in this chapter, because it is the approximation in our nonlinear model.

Of course, some other approximations and simplifications have been made, wherever necessary. These three distributions converge to each other as the number of measurements tends to infinity.

It may be helpful to describe the concepts of random and systematic errors before the introduction of normal distribution. If it is possible to get rid of the experimental uncertainties by repeating the measurements, these uncertainties are then called "random errors." Otherwise, they are said to be "systematic errors." As it can be noticed from the descriptions given above, the systematic errors can not be prevented completely, whereas there are some statistical methods which make it possible to reduce the random errors. But, it is possible to determine various sources of systematic errors and check whether they are small enough as warranted by the required precision level or not.

5.2 Nonlinear Models

Now, considering a model fitting that depends nonlinearly on a set of M unknown parameters a_k (k = 1,2...M), an attempt will be made to determine the set of best fit parameters by minimizing the χ^2 merit function which is a measure of the deviation between the fitted curve and the actual measurements.[14]

Denoting the model to be fitted as $y = y(x:a)$ (5.1)

where the vectors a, x stand for the parameter set and the

set of independent variables respectively, the χ^2 merit function is given by

$$\chi^2(a) = \sum_{i=1}^{N} \left[\frac{y_i - y(x_i;a)}{\sigma_i} \right]^2 \qquad (5.2)$$

Here χ^2 is a function of fit parameters a, $y(x_i;a)$ stands for the fitting function evaluated at values x_i of the independent variable for the same parameter set a and finally y_i are the experimentally measured values of the dependent variable for which the best fit is being sought.

The best fit parameters a will be determined by minimizing this χ^2 function with respect to a. For this purpose taking some particular point a as the origin of the coordinate system with coordinates a, any well behaved function can be approximated by a Taylor series expansion in the form:

$$f(a+\delta a) = f(a) + \sum_i \frac{df}{da_i} \delta a_i + \frac{1}{2} \sum_i \sum_j \frac{d^2 f}{da_i\, da_j} \delta a_i \delta a_j + \ldots \quad (5.3)$$

Truncation after the second degree term leads to the quadratic equation

$$f(a+\delta a) \approx c - b.\delta a + \frac{1}{2} \delta a.A.\delta a \qquad (5.4)$$

where A is called the "Hessian" or the second derivative matrix of the function evaluated at the point a. Now, using the procedure given above, the merit function can be approximated by a quadratic form similar to Eqn. (5.4) when it is sufficiently close to the minimum.

$$\chi^2(a+\delta a) \approx \tau - d_M . \delta a + \frac{1}{2} \delta a . A_{M \times M} . \delta a \quad (a_k,\ k=1,\ldots M) \qquad (5.5)$$

Setting the first derivative of equation (5.4) equal to zero with the purpose of minimization with respect to a gives;

$$A . a_{min} = b \qquad (5.6)$$

at its exact minimum. But at the current point of evaluation df/da is not exactly zero and

$$A . a_{cur} = \left. \frac{df(a)}{da} \right|_{a_{cur}} + b \qquad (5.7)$$

holds, where cur stands to represent the current values. Subtracting equations (5.6) and (5.7)

$$A(a_{min} - a_{cur}) = -\nabla f(a_{cur}) \qquad (5.8)$$

$$a_{min} - a_{cur} = A^{-1}[-\nabla f(a_{cur})]$$

Applying this to the case under consideration, Eqn. (5.8) is evaluated as;

$$a_{min} = a_{cur} + A^{-1}[-\nabla \chi^2(a_{cur})]. \qquad (5.9)$$

At the minimum point, a_{cur} converges to a_{min} at a single step.

On the other hand, the approximation procedure expressed by the quadratic expression (5.5), might be a poor local approximation to the shape of the function that is being minimized at a_{cur}. In that case, " the steepest descent method" is used to take a step down the gradient. In other words,

$$a_{next} = a_{cur} - \text{constant} \times \nabla \chi^2(a_{cur}) \qquad (5.10)$$

where the constant is a small number.

The gradient of the χ^2 function and the matrix A must be computed at the current set of parameters a in order to use equation (5.9) and (5.10). The form of χ^2 and its derivatives are known since χ^2 is based on a model function specified by us. Therefore both the Hessian matrix and the gradient of χ^2 can be evaluated at a_{cur}.

The gradient of χ^2 with respect to the parameters a which will be zero at the minimum of χ^2 has the components

$$\frac{dX^2}{da_k} = -2 \sum_{i=1}^{N} \frac{[y_i - y(x_i;a)]}{\sigma_i^2} \frac{dy(x_i;a)}{da_k} \qquad k=1,2,\ldots,M \qquad (5.11)$$

Taking an additional partial derivative gives

$$\frac{d^2X^2}{da_k\, da_l} = 2 \sum_{i=1}^{N} \frac{1}{\sigma_i^2} \left[\frac{dy(x_i;a)}{da_k} \frac{dy(x_i;a)}{da_l} - [y_i - y(x_i;a)] \frac{d^2y(x_i;a)}{da_l\, da_k} \right]$$

By defining

$$\beta_k \equiv -\frac{1}{2} \frac{dX^2}{da_k}\bigg|_{a_{cur}} \qquad \alpha_{kl} \equiv \frac{1}{2} \frac{d^2X^2}{da_k\, da_l}\bigg|_{a_{cur}} \qquad (5.12)$$

setting $[\alpha] = \frac{1}{2} A$ in equation (5.9), this equation can be rewritten as the set of linear equations

$$\sum_{l=1}^{M} \alpha_{kl}\, \delta a_l = \beta_k \qquad (5.13)$$

This set is solved for the increaments δa_l such that, when added to the current approximation will result in the next approximation.

On the other hand, equation (5.10) is transformed to

$$\delta a_l = \text{constant} \times \beta_l \qquad (5.14)$$

Determination of the constant in this iterative scheme requires further consideration and is based on no concrete rules but on expediency

5.2.1 Levenberg-Marquardt Method

The method is based on two elementary suggestions. There is no information about the constant and its magnitude in equation (5.14). According to Marquardt, the components of the Hessian matrix give some information about the order of magnitude.[14]

Considering equation (5.2) and the fact that σ_i is the standard deviation of y having the same dimension, it can be concluded that the quantity χ^2 is a dimensionless quantity. On the other hand, β_k have the dimensions of $1/a_k$. Therefore, the constant in equation (5.14) must have the dimension of a_k^2. The reciprocal of the diagonal element of $[\alpha]$, $1/\alpha_{kk}$, must set the scale of the constant since it has the dimensions of a_k^2. It is divided by a factor Ω since it might be too big for a desirable rate of convergence. Thus, equation (5.14) is replaced by the equation

$$\delta a_i = \frac{1}{\Omega a_{ii}} \beta_i \qquad (5.15)$$

Marquardt's second suggestion is that equations (5.13) and (5.15) can be combined by the definition of α'

$$\alpha_{jj}' \equiv \alpha_{jj}(1+\Omega) \qquad (5.16)$$

$$\alpha_{jk}' \equiv \alpha_{jk} \qquad (j \neq k)$$

and thus

$$\sum \alpha_{kl} \cdot \delta a_l = \beta_k \qquad (5.17)$$

The computational procedure may be outlined as follows: First a linear fit is made to obtain an initial guess for the parameters a, and $\chi^2(a)$ is computed for this set of parameters a, after which the linear equations given by Eqn. (5.17) are solved for δa and $\chi^2(a+\delta a)$ is computed using a modest value for Ω such as 0.001. If $\chi^2(a+\delta a) \geq \chi^2(a)$, Ω must be increased by a factor of 10 and calculations of the previous step must be performed for the current value of Ω. Conversely if $\chi^2(a+\delta a) < \chi^2(a)$, Ω is decreased and the trial solution is recalculated using $a+\delta a$ instead of a before going back to the previous step of recalculating the entries α_{kl} at the new $a+\delta a$ value. This procedure may be stopped on the first or second negligible decrease in χ^2. A decrement less than 0.1 or a fractional amount like 10^{-3} is suitable for this purpose.

5.2.2 Computational Procedure

Firstly, a linear least squares fit was performed by using the experimental data and putting the basic equation (4.1) into the linear form given by

$$\ln(I_o) - \ln(I) = \mu x \qquad (5.18)$$

This equation may be represented by the following simple mathematical model

$$y = A + B\,x \qquad (5.19)$$

where A, B and y correspond to ln(Io), μ and ln(I), respectively.

Parameters A, B were used to form an initial estimate for the nonlinear least squares fit. After the application of the iterative procedure outlined in the previous section we end up having the best nonlinear fit to $y=y(x_i;a)$. But now the problem is the determination of the error in the independent variable x as a function of the error in the dependent variable y. Note that the latter can be obtained from the set of measurements since y is the measured quantity. To this effect the variance σ_f^2 of any function can be computed by;

$$\sigma_f^2 = \sum_{i}^{N} \sigma_i^2 \left(\frac{df}{dy_i} \right)^2 \qquad (5.20)$$

Use will be made of this relationship in finding the aforementioned uncertainties.

Nonlinear curve fitting procedure uses the exponential mathematical model expressed as

$$y = A \exp(B\,x) \qquad (5.21)$$

In this equation, y and x represent count rate and the thickness of the sample respectively. Using the A and B values calculated by the linear curve fitting procedure described above, it is only possible to calculate the logarithms of count rate values for several thicknesses. Obviously, this would not be physically significant. Taking the exponents of these logarithmic terms will not give the same result that a nonlinear curve fitting would, because

that would be a different mathematical procedure . In other words, it is necessary to perform a nonlinear curve fit in order to make the interpretation of data possible. Nevertheless, a linear least squares curve fit was initially performed to form a good initial estimate for the nonlinear curve fitting as it was mentioned above.

In our case, the merit function is

$$\chi^2(A,B) = \left[\frac{y_i - (A\, e^{Bx})}{\sigma_i}\right]^2 \qquad (5.22)$$

Using the iterative procedure described above, the parameters minimizing χ^2 and their uncertainties are calculated. However, uncertainties in x and y values are more interesting than those of A and B since they have physical meanings. Uncertainty in y can be computed using the following expression.

$$\sigma_y^2 = \sigma_A^2 \left(\frac{dy}{dA}\right)^2 + \sigma_B^2 \left(\frac{dy}{dB}\right)^2 + 2\,\sigma_{AB} \left(\frac{dy}{dA}\right)\left(\frac{dy}{dB}\right) \qquad (5.23)$$

Since the fitted function is in the form of y = y(x), an inverse relation is needed to find the uncertainty in x. This relation is given as

$$\left|\frac{dy}{dx}\right| \sigma_x = \sigma_y$$

or (5.24)

$$\sigma_x = \sigma_y \left|\frac{dy}{dx}\right|^{-1}$$

This uncertainty in x is caused by the uncertainties in the parameters of curve fitting and must be considered separately

from the uncertainty caused by statistical distribution of measurement points, that is given as

$$\sigma_y = \left[\frac{\sum_{i=1}^{N} (y_i - \bar{y})^2}{N-1} \right]^{\frac{1}{2}} \qquad (5.25)$$

where N is the number of the experimental data points. Finally then σ_x can be computed by using σ_y evaluated as such.

The results of these error analysis calculations are reproduced in table 5.1. for a sample set of data in order to give an idea of the magnitudes involved.

Table 5.1. Sample output of curve fitting procedure

Thickness (mg/cm^2)	Counts (cpm)	Calculated (cpm)	σ_i (cpm)	σ_y (cpm)	σ_x (mg/cm^2)
0.000	186332	198212	57	193	0.330
18.823	181076	186831	46	274	0.482
37.429	174370	176224	38	46	0.084
55.931	167278	166274	31	125	0.237
74.421	159528	156891	26	199	0.396
92.981	151544	148047	23	118	0.247
111.362	143006	139702	22	53	0.118
129.829	134772	131828	23	186	0.438
148.295	126659	124398	24	41	0.103
166.756	118724	117389	26	112	0.300
185.207	110275	110779	29	161	0.466
203.556	102598	104574	30	89	0.275
221.985	95328	98692	33	140	0.467
240.323	88026	93167	35	93	0.365
258.613	81142	87965	37	169	0.510
276.868	74472	83062	38	119	0.531

A=198212 B=-0.003141 for $y=A\exp(Bx)$

VI. DISCUSSION AND CONCLUSIONS

In this study, a prototype radio gauge was developed to measure the thickness of paper sheets by using a charged particle source. The unknown mass thickness values were found by using calibration curves which had been drawn from the experimental data. A data base was prepared for a wide range of paper thicknesses to obtain the calibration curves.

It is well known that as a preliminary step, a suitable source is chosen considering the properties of the sample material by using the equation expressed as $\mu x=2$. Given the thickness of sample material, a source that gives a value close to that of μ would be the most suitable one. If there is a limitation in the choice of source such as high cost, rare isotope or difficulty in handling, then a suitable thickness range is determined for the sample material and source being used. The major aim in the experiments, was to determine the unknown paper thicknesses for static and dynamic systems by using a Sr^{90} source. Since the sample material and source were defined initially, the problem was reduced to determination of the suitable thickness. Considering that the end point energy of this isotope is about 2.24[15] Mev and the mass thickness of a paper sample may be quite low depending on the composition, it is obvious that the suitable thickness values for this purpose would be quite large. It may only be possible to obtain these required thicknesses by using a thick pile of paper sheets. However, these varying thickness values from

a very thin paper layer to an extremely thick pile changes the geometry of the system and causes gradually increasing numbers of undesirable scatterings. Measurements near the maximum range are quite difficult to perform because of these scattered particles. To prevent these scatterings caused by the thick sample material, a careful collimation is needed on the detector side. However, as it was explained in the experimental procedure, the samples must be located as close as possible to detector to reduce the scatterings caused by the target holder. Therefore, it could not be possible to prevent the scattering effect completely. In the experiments, an attempt was made to collimate the beam coming on to the detector considering the geometrical limitations.

Activity of the source used is about 3 mCi. Obviously, this activity is quite high for this type of measurements. Considering this fact this value was reduced by increasing the source detector distance. Since our experimental system was not in a vacuum tube, several types of interactions between the air molecules and beta particles were taking place. Another source of uncertainty is born out of the probabilistic nature of these interactions. Also, high source activity made the use of a shield mandatory but since induced X rays were produced by the energetic particles in the lead shield material, a further lead shield was constructed between the source and the observer. However, it was seen that the amount of induced X rays was not negligible even under these conditions. Of course, some of these scatterings were caused by the scaled box used to obtain a rigid system.

Another problem encountered during the experiments was caused by the changing level of humidity in the sample sheets depending on that of the surrounding area. It was therefore clear that all the sample sheets had to be kept under similar conditions. But because weighing all the samples would be a time consuming additional task this precaution proved to be difficult to meet satisfactorily. Hence interpretation of the measurements was done by using the values of a calibration curve obtained from samples under different ambient conditions.

It is well known that the thickness measurements performed by using a radio gauge are non-destructive and no contact is required with the material during the measurements. Therefore, radio gauge applications are suitable especially for on-line thickness measurements but the observation period must be very small to perform the dynamic measurements. However, it was decided to use a 60 second observation period to reduce the statistical errors. It was also concluded that the type of the detection system and activity level of the source were not suitable for the on-line measurements.

The following procedure is therefore suggested to measure the thickness of paper samples more accurately: Firstly, a suitable source must be chosen by using the appropriate expressions. Of course, the suitable source energy would be lower than the one used in this study. A C^{14} source of ≈0.155 Mev energy level[15] is quite suitable for measuring the thickness of thin paper sheets. It is clear

that, a vacuum chamber is necessary for this low energy level and the required activity is less than 10 μCi. If the system is not in a vacuum tube however, a higher activity level may be needed in which case there would be no need to shield the system.

APPENDIX

THICKNESS (mg/cm²)	COUNTS (cpm)	CALCULATED VALUES (cpm)
0.000	190600	199571
18.824	185264	188593
37.549	178238	178272
56.274	170838	168515
74.951	163751	159315
93.578	155587	150640
112.206	147595	142438
130.833	139273	134682
149.362	131503	127386
167.892	123215	120485
186.421	115109	113958
204.951	107591	107784
223.382	100072	101976
241.813	92669	96480
260.146	85619	91307
278.431	78845	86424

199571.48 B=0.00300579 $Y = A \exp(-BX)$

and B were determined by using a nonlinear curve fitting procedure

Regression Output for $Y = A + B X$

Constant A :	203920.6
B Coefficient:	-0.00319
Std Err of B :	0.000106

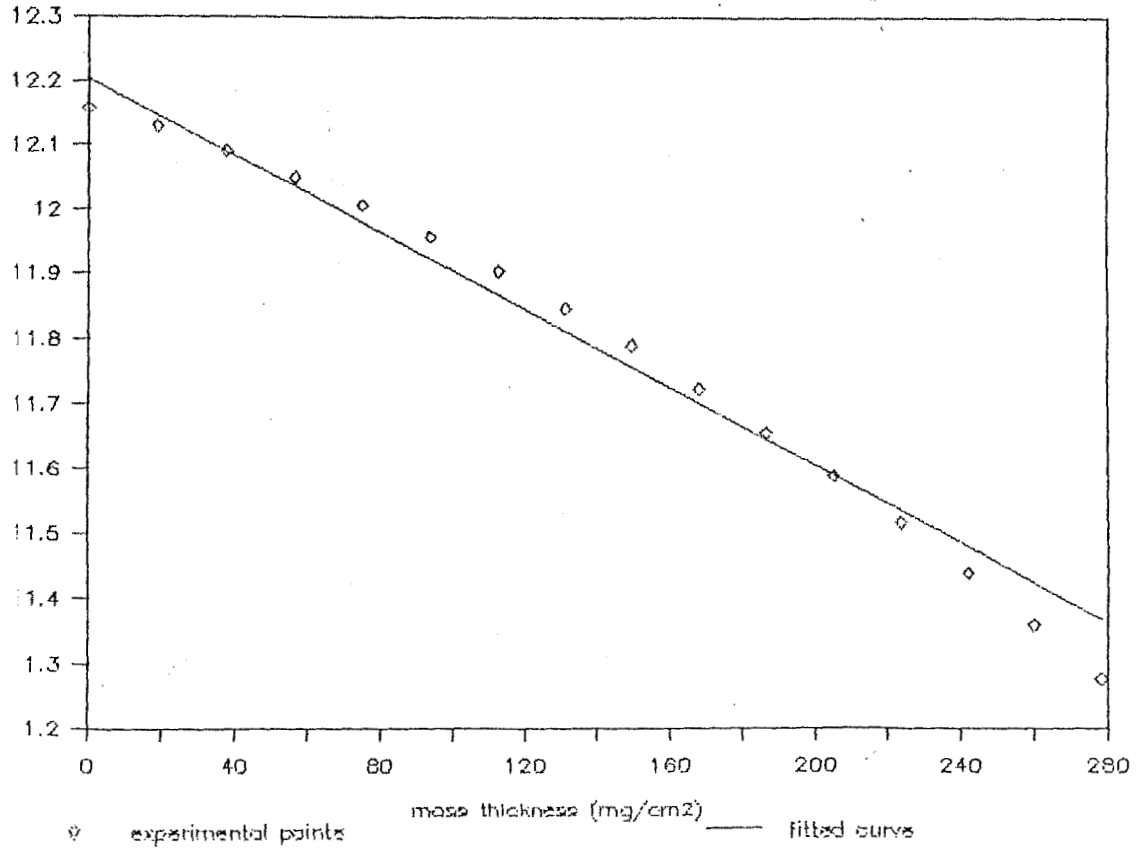

THICKNESS (mg/cm²)	MEASURED COUNTS (cpm)	COUNTS CALCULATED (cpm)
0	188196	272282.7
216.1085	96136	77275.44
323.6198	55968	41297.75
431.0201	30647	22084.74
538.6102	14262	11797.16
648.6671	5588	6211.832
756.5404	2014	3312.748
871.925	990	1691.008
987.3096	794	863.1835
1096.797	792	456.0222

Regression Output:

Std Err of Y Est		0.399541
Coefficient	B	-0.00582
Constant	A	272282.7

$$y = A + Bx$$

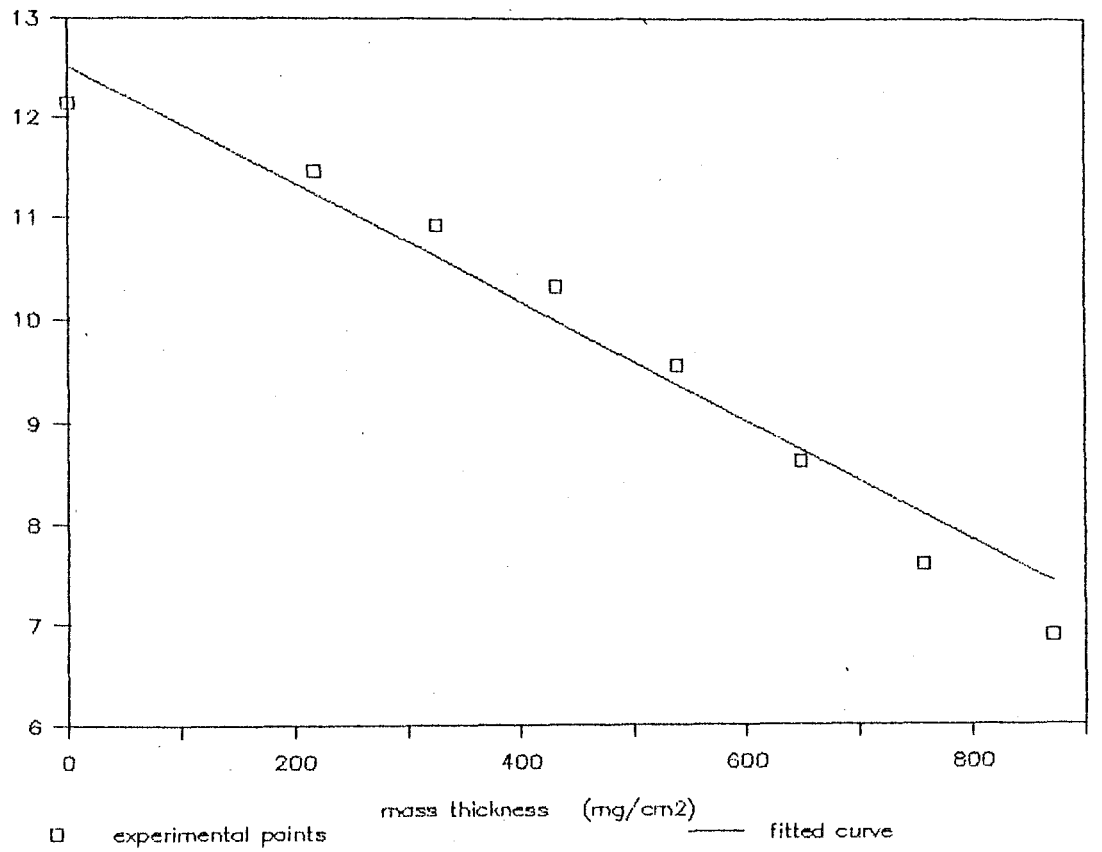

REFERENCES

1- Cameron, J.F., and Clayton, C.G., Radioisotope Instruments, V.1, Pergamon Press, 1971.

2- Evans, R.D., The Atomic Nucleus, New York: Mc Graw-Hill Book Comp. Inc., 1955.

3- Gardner, R.P., Ely, R.L.Jr., Radioisotope Measurement Applications in Engineering, New York: Reinhold, 1967.

4- Katz, L., Penfold, A.S., "Range-Energy Relations for Electrons.," Reviews of Modern Physics, Vol. 24, No 1, pp 28-44, 1952.

5- Thontadarya, S.R.,"Effect of Geometry on Mass Attenuation Coefficient of -Particles," Int. J. Appl. Radiat. Isot., Vol. 35, No 10, pp 981-982, 1984.

6- Thontadarya, S.R., " Determination of Range of Beta Particles in Aluminum from Their Mass Attenuation Coefficients," Int. J. Appl. Radiat. Isot.,Vol. 36, No 3, pp 251-252, 1985.

7- Knoll, G.F., Radiation Detection and Measurement, New York: John Willey and Sons, 1979.

8- Bilge, A.N., Nükleer Tekniklerin Endüstriye Uygulanması, T.A.E.K., 1985.

9- Glasstone, S., Sesonke, A., Nuclear Reactor Engineering, New York: D.Van Nostrand, 1964.

10- Borak, F., Nuclear Engineering Laboratory Notes, B.U., 1982.

11- Oyedele, J.A., "Dynamic Effect in On-line Thickness Measurement Employing Radiation Beams," Int. J. Appl. Radiat. Isot., Vol. 38, No 7, pp 527-533, 1987.

12- Oyedele, J.A., "Source Fluctuation Effect in Continuous Radiogauging," Int. J. Appl. Radiat. Isot., Vol. 39, No 9, pp 981-986, 1988.

13- Taylor, J.R., An Introduction to Error Analysis, University Science Books, 1982.

14- Press, W.H., Flannery, B.P., Teukolsky, S.A., and Vetterling,W.T., Numerical Recipes, Cambridge University Press, 1986.

15- Lederer, C.M., Hollander, J.M., Perlman,I., Table of Isotopes, New York: John Willey and Sons, 1967.